Inorganic Chemistry

Article

pubs.acs.org/IC

Impact of Coordination Geometry, Bite Angle, and Trans Influence on Metal−Ligand Covalency in Phenyl-Substituted Phosphine Complexes of Ni and Pd

Courtney M. Donahue,[†] Samuel P. McCollom,[‡] Chelsie M. Forrest,[§] Anastasia V. Blake,[†] Brian J. Bellott,[§] Jason M. Keith,*[,‡] and Scott R. Daly*[,†]

[†]Department of Chemistry, The University of Iowa, E331 Chemistry Building, Iowa City, Iowa 52242, United States

[‡]Department of Chemistry, Colgate University, 13 Oak Drive, Hamilton, New York 13346, United States

[§]Department of Chemistry, Western Illinois University, 1 University Circle, Macomb, Illinois 61455, United States

Supporting Information

ABSTRACT: Despite the long-standing use of phosphine and diphosphine ligands in coordination chemistry and catalysis, questions remain as to their effects on metal−ligand bonding in transition metal complexes. Here we report ligand K-edge XAS, DFT, and TDDFT studies aimed at quantifying the impact of coordination geometry, diphosphine bite angle, and phosphine trans influence on covalency in M−P and M−Cl bonds. A series of four-coordinate $NiCl_2$ and $PdCl_2$ complexes containing PPh_3 or $Ph_2P(CH_2)_nPPh_2$, where n = 1 (dppm), 2 (dppe), 3 (dppp), and 4 (dppb), was analyzed. The XAS data revealed that changing the coordination geometry from tetrahedral in $Ni(PPh_3)_2Cl_2$ (**1**) to square planar in $Ni(dppe)Cl_2$ (**2**) more than doubles the intensity of pre-edge features assigned to Ni−P and Ni−Cl 1s → σ^* transitions. By way of comparison, varying the diphosphine in $Pd(dppm)Cl_2$ (**4**), $Pd(dppp)Cl_2$ (**6**), and $Pd(dppb)Cl_2$ (**7**) yielded Pd−P 1s → σ^* transitions with identical intensities, but a 10% increase was observed in the P K-edge XAS spectrum of $Pd(dppe)Cl_2$ (**5**). A similar observation was made when comparing $Ni(dppe)Cl_2$ (**2**) to $Ni(dppp)Cl_2$ (**3**), and DFT and TDDFT calculations corroborated XAS results obtained for both series. Comparison of the spectroscopic and theoretical results to the diphosphine structures revealed that changes in M−P covalency were not correlated to changes in bite angles or coordination geometry. As a final measure, P and Cl K-edge XAS data were collected on *trans*-$Pd(PPh_3)_2Cl_2$ (**8**) for comparison to the cis diphosphine complex $Pd(dppe)Cl_2$ (**5**). Consistent with phosphine's stronger trans influence compared to chloride, a 35% decrease in the intensity of the Pd−P 1s → σ^* pre-edge feature and a complementary 34% increase in Pd−Cl 1s → σ^* feature was observed for **8** (trans) compared to **5** (cis). Overall, the results reveal how coordination geometry, ligand arrangement, and diphosphine structure affect covalent metal−phosphorus and metal−chloride bonding in these late transition metal complexes.

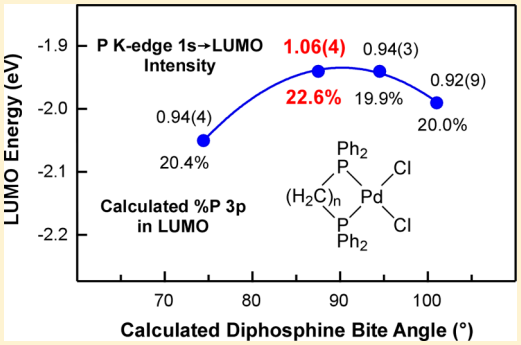

INTRODUCTION

Diphosphine ligands offer remarkable versatility in transition metal catalysis: their substituents and structures can be modified to influence the rates of chemical reactions, tune the electronic properties of metals, and affect the stereochemistry of catalytic products.[1] Given the myriad of possibilities for phosphine and diphosphine derivatization,[2] there have been numerous efforts to understand how electronic and structural variations at phosphorus contribute to fundamental differences in catalytic performance.[3−8] Notable among these are the seminal contributions of Tolman, who provided structural and electronic parameters that are still used to inform the design of metal phosphine complexes.[9,10] In general, these efforts continue to evolve and are driven by a need to develop metrics that can be used to identify phosphine ligands that enhance the performance and selectivity of homogeneous catalysts.[11−16]

A parameter that has been used extensively to correlate reactivity in diphosphine complexes is bite angle.[17−21] The bite angle (β), defined as the P−M−P angles in diphosphine complexes,[22] can have a pronounced effect on the rates of catalytic reactions.[19−21,23−28] Changes in reaction rates are often attributed to a diphosphine's ability to stabilize transition-state geometries or impart steric strain,[29−35] but questions remain as to how reactivity may be affected by structure-induced differences in metal−diphosphine bonding and electronic structure.[28] Furthermore, metal−phosphorus bonds contain a mixture of covalent, electrostatic, and repulsive interactions that are difficult to distinguish experimentally.[36] Much of what is known comes from spectroscopic,[37−42] electrochemical,[43−45] and theoretical[46,47] investigations of

Received: December 31, 2014
Published: May 21, 2015

ACS Publications © 2015 American Chemical Society

DOI: 10.1021/ic503125b
Inorg. Chem. 2015, 54, 5646−5659

diphosphine bite angle effects on molecular orbital energies. Walsh diagrams are often used to illustrate and account for changes in the orbital energies as a function of diphosphine structure and coordination geometry.[23,42,48,49]

While it is known that changes in diphosphine bite angle can have a pronounced influence on molecular orbital energies, it is not clear how these energy variations relate to changes in M−P orbital mixing. To understand the interplay between diphosphine structure and covalent M−P bonding, we are using ligand K-edge X-ray absorption spectroscopy (XAS) to evaluate how M−P orbital mixing (i.e., covalency) in late transition metal complexes is affected by changes in coordination geometry and diphosphine structure. As reviewed by Solomon and co-workers,[50] ligand K-edge XAS uses synchrotron-generated X-rays to probe electronic transitions between 1s core orbitals localized on ligand donor atoms and singly occupied or unoccupied molecular orbitals (MOs) containing ligand p character and (predominately) metal d character. The presence of ligand p character in the associated wave functions results in dipole-allowed transitions (1s → np) with transition intensities governed by the amount of ligand p-orbital mixing. As a result, the intensity of these XAS features is known to provide a good estimate of ground-state metal−ligand covalency (as defined by Heitler and London) for bonds involving p orbitals on the ligands.[50−53] While ligand K-edge XAS has been used extensively and is now relatively common for studying bonding in metal complexes containing Cl and S ligands,[50,52−60] it has only recently been used to investigate covalency in metal−phosphorus bonds.[61−63]

Here we report the first P K-edge XAS investigation of stereoelectronic contributions to M−P covalency in diphosphine complexes. P K-edge XAS data were collected on a series of $NiCl_2$ and $PdCl_2$ complexes with the phosphine and diphosphine ligands PPh_3, dppm, dppe, dppp, and dppb (Figure 1). These complexes were selected to analyze how

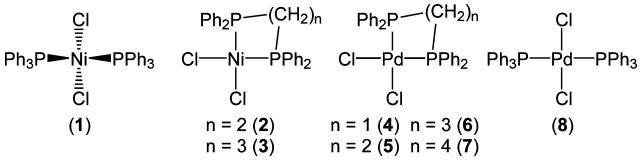

Figure 1. Numbering scheme for phosphine and diphosphine complexes investigated by XAS.

changes in coordination geometry (tetrahedral vs square planar) and diphosphine bite angle affect M−P covalency. Chloride was selected as the ancillary ligand so that we could collect Cl K-edge XAS data to determine how the structural variations affect metal−ligand bonding at coordination sites trans to the M−P bonds. In addition to exploring bite angle effects, the studies provided an opportunity to examine the impact of the trans influence on metal−ligand covalency in related cis and trans $PdCl_2$ complexes. The ligand K-edge XAS experiments were supported by DFT and TDDFT calculations and by additional XAS experiments at the Pd L_2- and L_3-edges. As we will show, the results demonstrate how ligand K-edge XAS and complementary DFT and TDDFT calculations can be used to quantify changes in phosphine structure and coordination environment on M−P orbital mixing.

EXPERIMENTAL SECTION

Synthesis of Phosphine and Diphosphine Complexes. Crystalline samples of $Ni(PPh_3)_2Cl_2$ (**1**), $Ni(dppe)Cl_2$ (**2**), $Pd(dppm)Cl_2$ (**4**), $Pd(dppe)Cl_2$ (**5**), $Pd(dppp)Cl_2$ (**6**), $Pd(dppb)Cl_2$ (**7**), and *trans*-$Pd(PPh_3)_2Cl_2$ (**8**) were prepared using established literature methods.[64−66] The identity and purity of the compounds were confirmed by ^1H and ^{31}P NMR spectroscopy. $Ni(dppp)Cl_2$ (**3**) was purchased from Strem and used as received. Because it has been proposed that polymeric structures of $Pd(dppb)Cl_2$ (**7**) are possible,[67] powder XRD data was collected on **7** to confirm that the crystallographic parameters matched those for the monomeric structure. As shown in Figure S13 (Supporting Information), the powder XRD pattern for the XAS sample is in agreement with the calculated powder pattern from the single-crystal XRD of monomeric **7**.[68]

XAS Sample Preparation. XAS samples prepared in air were done as previously described.[59] In one study, the Pd complexes **4**−**7** were analyzed in the absence of air by preparing the samples in a N_2 glovebox. Each sample was sealed using a polypropylene window adhered to the aluminum block using double-sided tape. The samples were removed from the glovebox in a sealed glass container and transported to a glovebag attached to the beamline sample chamber. Once the glovebag was purged for at least 30 min, the sample was transferred into the sample chamber. XAS data revealed no differences compared to those for samples prepared in air.

XAS Data Collection. All XAS data were collected at the Stanford Synchrotron Radiation Lightsource (SSRL). Cl K-edge and Pd $L_{2/3}$-edges were collected on Beamline (BL) 4-3, which is equipped with a 20-pole, 2.0 T wiggler and double-crystal monochromator cooled with liquid nitrogen. P K-edge data were collected on BL14-3, which has a bending magnet source and a water-cooled double-crystal monochromator. The sample chamber was maintained under a He atmosphere at room temperature, and fluorescence was measured using a PIPS detector on both beamlines. P K-edge XAS data were calibrated by setting the maximum of the second pre-edge feature of a $Na_4P_2O_7$ standard to 2152.40 eV and applying the same shift to subsequent sample scans. Similarly, Cs_2CuCl_4 was used as the calibration standard for Cl K-edge and Pd $L_{2/3}$-edge spectra by setting the maximum of the first pre-edge feature to 2820.20 eV. Data were collected in sets of three for each sample during a run, and a calibration scan was collected before and after each sample set.

Data were collected over three regions in the P and Cl K-edge XAS experiments. P K-edge data were collected with 1.0 eV steps and 1 s dwell times between 2106 and 2136 eV (pre-edge), 0.08 eV steps and 1−2 s dwell times between 2136.08 and 2180 eV (edge), and 1.5 eV steps and 1 s dwell times between 2181.5−2381 eV (postedge). Cl K-edge data points were collected with 1.0 eV steps and 1 s dwell times between 2700−2815 eV (pre-edge), 0.08 eV steps and 1 or 2 s dwell times between 2815.08 and 2840 eV (edge), and 1.5 eV steps and 1 s dwell times between 2841.5 and 3050 eV (postedge). Pd L_2- and L_3-edge data were collected in tandem with 1.5 eV steps and 1 s dwell times between 2841.5 and 3060 eV, 0.8 eV steps with 1s dwell times between 3160.08−3190 eV, 1.5 eV steps with 1 s dwell times between 3191.5−3315 eV, 0.8 eV steps with 1 s dwell times between 3315.08 and 3333.45 eV, and 1.5 eV steps 1 s dwell times between 3346.5 and 3501 eV. In some experiments, Cl K-edge data for the Pd phosphine complexes **4**−**8** were collected in tandem with the Pd L_2- and L_3-edges at higher energy.

XAS Data Analysis. All calibrations, background subtractions, normalizations, and averaging were performed using the Athena program in the IFFEFIT XAS software package.[69] The background was removed from each spectrum by fitting a first-order polynomial to the pre-edge region. The P K-edge XAS data was normalized by fitting the postedge region with a first-order polynomial and setting the step function to an intensity of 1.0 at a set point of 2165 eV. The Cl K-, Pd L_3-, and Pd L_2-edge data were normalized by fitting the postedge regions with second-order polynomials. The step functions were set to an intensity of 1.0 at set points of 2840 (Cl K), 3195 (Pd L_3), and 3345 eV (Pd L_2).

DOI: 10.1021/ic503125b
Inorg. Chem. 2015, 54, 5646−5659

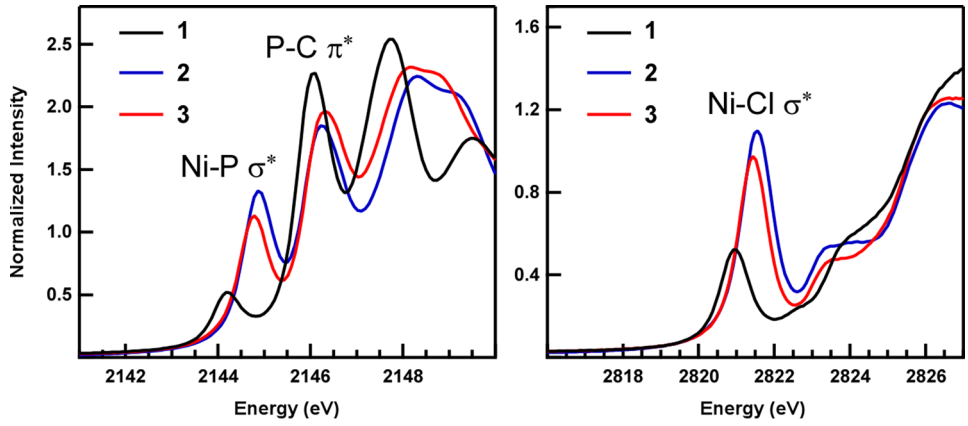

Figure 2. Normalized and background-subtracted P K-edge (left) and Cl K-edge (right) XAS spectra for $Ni(PPh_3)_2Cl_2$ (**1**; black), $Ni(dppe)Cl_2$ (**2**; blue), and $Ni(dppp)Cl_2$ (**3**; red).

Fits to the spectra were performed with the IGOR Pro 6.3 software program using a modified version of EDGEFIT.[50] The data were modeled using curves with a 1:1 Lorentzian/Gaussian mixture. The number of curves used and their positions were determined using the minima in second-derivative traces of the spectra. Curves were fit over a range from 2140 to 2150 eV for P K and from 2819 to 2830 eV for Cl K. Curve-fit intensities were calculated by multiplying the height by the full width at half max (fwhm), as described previously.[50]

DFT and TDDFT Calculations. All theoretical calculations were performed with the Gaussian09 computational chemistry suite.[70] Ground-state geometries and electronic structures were optimized in the gas phase at the hybrid density functional level with the three-parameter exchange functional of Becke and the correlation functional of Lee, Yang, and Parr comprising the B3LYP functional.[71,72] For the high-spin Ni compounds unrestricted calculations were performed, which results in a separate density matrix for the α and β electrons that are allowed to differ resulting in α and β spin-orbitals. Pd and Ni were modeled with the effective core potential of Hay and Wadt with the associated uncontracted basis set collectively known as LANL08.[73,74] All other atoms were modeled with Pople's valence double-ζ 6-31G** basis set.[75,76] While this functional is likely the source of the inconsistencies between the experimental and the theoretical structures, this functional and basis set combination has demonstrated good agreement with ligand K-edge XAS data for inorganic systems.[52,53,57−60] In addition we found that inclusion of Gimme's d3 empirical dispersion corrections in related systems result in better agreement with experimental geometries but have no apparent effect on the overall TDDFT-generated spectra. The M, P, and Cl s, p, and d orbital participation was determined by Mulliken population analysis on the individual Kohn−Sham orbitals.

Theoretical spectra were simulated using time-dependent density functional theory (TDDFT). These calculations were performed as previously described[52,57−60] and rely on the mixing between the core orbitals and the unoccupied frontier orbitals. The simulation involves a linear response calculation resulting in the transition energies and amplitudes between the ground state and the calculated excited states.[77] The transitions from occupied orbitals other than the Cl or P 1s were excluded so that only excitations relating to the Cl or P core to the virtual orbitals were observed. This prevents relaxation from occupied orbitals due to the core hole while allowing relaxation of the virtual orbitals. There are potentially two main areas of error associated with these TDDFT-generated final states. (1) When examining systems with unpaired electrons these methods fail to accurately model all of the various multiplets and instead give an average over some of the final states. This has been discussed previously and is not an issue in the closed shell systems examined in this work.[52,53,58] (2) When examining excitations of core electrons from chemically equivalent atoms in a molecule, such as those discussed in this manuscript, the resulting core hole is necessarily delocalized and overall the broken symmetry solutions with localized core holes are not properly evaluated. These broken symmetry solutions would likely have a small energy difference. The exact final states of the molecule, however, must have the overall symmetry of the molecule despite the fact that the individual spin-orbitals do not. One way to accurately handle this would be to take linear combinations of the broken symmetry final state solutions. These final states with the correct symmetry would necessarily have an even smaller energy difference. Alternatively, starting at the delocalized molecular orbital limit would require an expensive configuration interaction to arrive at the same solution.[78] By ignoring the broken symmetry final states there are two consequences. First, we see an average of these final states and do not observe the proper splitting of terms. Second, we see an error in the overall energy of all of the excitations due to the nonlocal nature of the core hole and inability to model the relaxation of the occupied orbitals. Despite these potential sources of error in this work, as well as in most of our previous work,[52,53,57−60] these methods still produce results that are in agreement within the resolution of the experiment except for an overall shift of the transition energies (i.e., the theoretical results are within the precision of the experiment despite some inaccuracy). A recent exception to this is the calculation of lanthanide M-edges in $LnCl_6^{2-}$ compounds where higher level theory was required to accurately model the spectroscopy.[53] As previously discussed,[52,53,57−60] an energy shift was applied to account for the errors in the accuracy of the simulated spectra in including these errors as well as errors associated with relativistic effects and general inaccuracy of the functional. This was accomplished by shifting the simulated transitions associated with the metal *n*d orbitals (Ni n = 3, Pd n = 4) to align with the corresponding experimental values. A shift of +49.9 eV for P and +64.3 eV for Cl was applied to the calculated spectra of tetrahedral **1**, and a shift of +49.6 eV for P and +64.6 eV for Cl was applied to square planar **2** and **3**. The Pd complexes (**4**−**8**) were shifted by 64.8 eV for Cl K-edge and 49.9 eV for P K-edge spectra. Individual excitations were identified by examination of the natural transition orbitals (NTOs).[79]

RESULTS

Ligand K-Edge XAS of Ni Phosphine Complexes. To demonstrate P K-edge XAS capability at the newly established Beamline 14-3 at the Stanford Synchrotron Radiation Lightsource (SSRL), we first analyzed tetrahedral $Ni(PPh_3)_2Cl_2$ (**1**) and square planar $Ni(dppe)Cl_2$ (**2**). Changing the molecular geometry in four-coordinate transition metal complexes is known to have a pronounced effect on M−Cl covalency,[50] but its impact on M−P bonding has not been explored by similar methods. XAS data were also collected on square planar $Ni(dppp)Cl_2$ (**3**) to quantify changes due to bite angle when exchanging dppe in **2** for dppp. The background-subtracted and normalized P and Cl K-edge XAS spectra for all three

DOI: 10.1021/ic503125b
Inorg. Chem. 2015, 54, 5646−5659

Table 1. Peak Positions and Intensities from P and Cl K-Edge XAS Data and TDDFT Calculations

	P K					Cl K				
compound	second deriv	curve fit	int	TDDFT	f^a	second deriv	curve fit	int	TDDFT	f^a
$Ni(PPh_3)_2Cl_2$ (**1**)	2144.2	2144.2	0.32(3)	2144.1	0.0010	2820.9	2821.0	0.43(2)	2820.9	0.0012
	2146.0	2146.1	1.3(1)	2146.0						
	2147.8	2147.7		2147.7						
	2149.5	2149.6		2149.9						
$Ni(dppe)Cl_2$ (**2**)	2144.9	2144.9	0.92(3)	2145.0	0.0022	2821.6	2821.5	1.02(2)	2821.6	0.0029
	2146.1	2146.2	1.6(1)	2146.1						
	2148.1	2148.2		2147.8						
	2149.3	2149.3		2148.9						
$Ni(dppp)Cl_2$ (**3**)	2144.8	2144.8	0.76(1)	2144.9	0.0021	2821.4	2821.4	0.91(6)	2821.5	0.0023
	2146.2	2146.3	1.4(1)	2146.2						
	2148.0	2148.0		2147.7						
	2148.9	2148.8		2149.0						
$Pd(dppm)Cl_2$ (**4**)	2145.3	2145.4	0.94(4)	2145.5	0.0022	2821.8	2821.8	1.00(4)	2821.6	0.0032
	2146.4	2146.4	1.7(2)	2146.2						
	2148.5	2148.5		2148.5						
	2149.5	2149.7		2149.5						
$Pd(dppe)Cl_2$ (**5**)	2145.4	2145.4	1.06(4)	2145.4	0.0026	2821.8	2821.7	1.13(5)	2821.7	0.0032
	2146.5	2146.5	1.7(2)	2146.4						
	2148.4	2148.4		2146.6						
	2149.4	2149.4		2148.3						
				2149.3						
$Pd(dppp)Cl_2$ (**6**)	2145.2	2145.2	0.94(3)	2145.4	0.0024	2821.6	2821.6	1.14(6)	2821.6	0.0036
	2146.4	2146.5	1.6(1)	2146.3						
	2148.1	2148.1		2148.1						
	2149.2	2149.1		2149.4						
$Pd(dppb)Cl_2$ (**7**)	2145.1	2145.2	0.92(9)	2145.3	0.0022	2821.5	2821.5	1.12(5)	2821.6	0.0035
	2146.4	2146.5	1.5(2)	2146.2						
	2148.2	2148.2		2146.8						
	2149.1	2149.0		2148.1						
				2149.2						
$Pd(PPh_3)_2Cl_2$ (**8**)	2145.1	2145.1	0.68(4)	2144.9	0.0019	2821.5	2821.5	1.51(3)	2821.9	0.0035
	2146.2	2146.2	1.6(2)	2146.3						
	2147.2	2148.4		2148.5						
	2148.3	2148.8		2149.5						
	2148.8									

[a]Sum of calculated oscillator strength (TDDFT) for all transitions associated with the first P and Cl K-edge XAS feature in each spectrum.

complexes are provided in Figure 2. These spectra are truncated, showing the most important features; full spectra can be found in the Supporting Information (Figure S1).

The P K-edge XAS spectrum for **1** has four resolved peaks, while the spectra of **2** and **3** have two resolved peaks at low energy and a broad third feature at higher energy. As reported for other d^8 complexes,[50,54,80] the lowest energy feature in each spectrum can be assigned to transitions associated with Ni−P bonds (1s → SOMO or 1s → LUMO), whereas higher energy features are assigned to antibonding MOs localized on the phosphine ligands. Overall, the greatest differences among all three spectra are found in the energy and intensity of the first peak (Table 1). The energy of the first feature in tetrahedral **1** is 2144.2 eV, which is 0.6−0.7 eV lower in energy than those in square planar **2** (2144.9 eV) and **3** (2144.8 eV). By comparison, the second features in these three spectra are relatively close to each other in energy (2146.0−2146.2 eV).

As observed in the P K-edge data, the Cl K-edge XAS spectra of **1**−**3** each reveal one dominant pre-edge feature. Each feature is again assigned to 1s → SOMO (**1**) or 1s → LUMO (**2** and **3**) transitions, the key difference being that they reflect Cl 3p character in the orbitals. Weaker pre-edge features between 2823 and 2825 eV are also present, but they are less pronounced compared to higher energy ligand transitions found in the P K-edge spectra. The first Cl K-edge peak for **1** (2820.9 eV) is 0.5−0.7 eV lower in energy than those of **2** (2821.6 eV) and **3** (2821.4 eV), which closely matches the trend observed in the P K-edge data.

To quantify the intensity of the pre-edge features, the P and Cl K-edge XAS spectra for **1**−**3** were modeled with pseudo-Voigt functions containing a 1:1 mixture of Lorentzian and Gaussian line shapes, as described previously (Figure 3).[50,59] The number of curves required to model each spectrum were determined initially by the number of minima in the second-derivative traces (Figure S2, Supporting Information). Peak positions obtained from refinement of the curve-fitting models are consistent with those obtained from the derivative traces of each spectrum (Table 1). Intensity values for each pre-edge position were obtained by taking the product of the modeled amplitude and the peak widths at half-maximum.[50] Errors bars for the modeled intensity were determined by having at least two people independently background subtract, normalize, average (3 scans), and curve-fit a minimum of two data sets obtained on different samples. This method provided a

DOI: 10.1021/ic503125b
Inorg. Chem. 2015, 54, 5646−5659

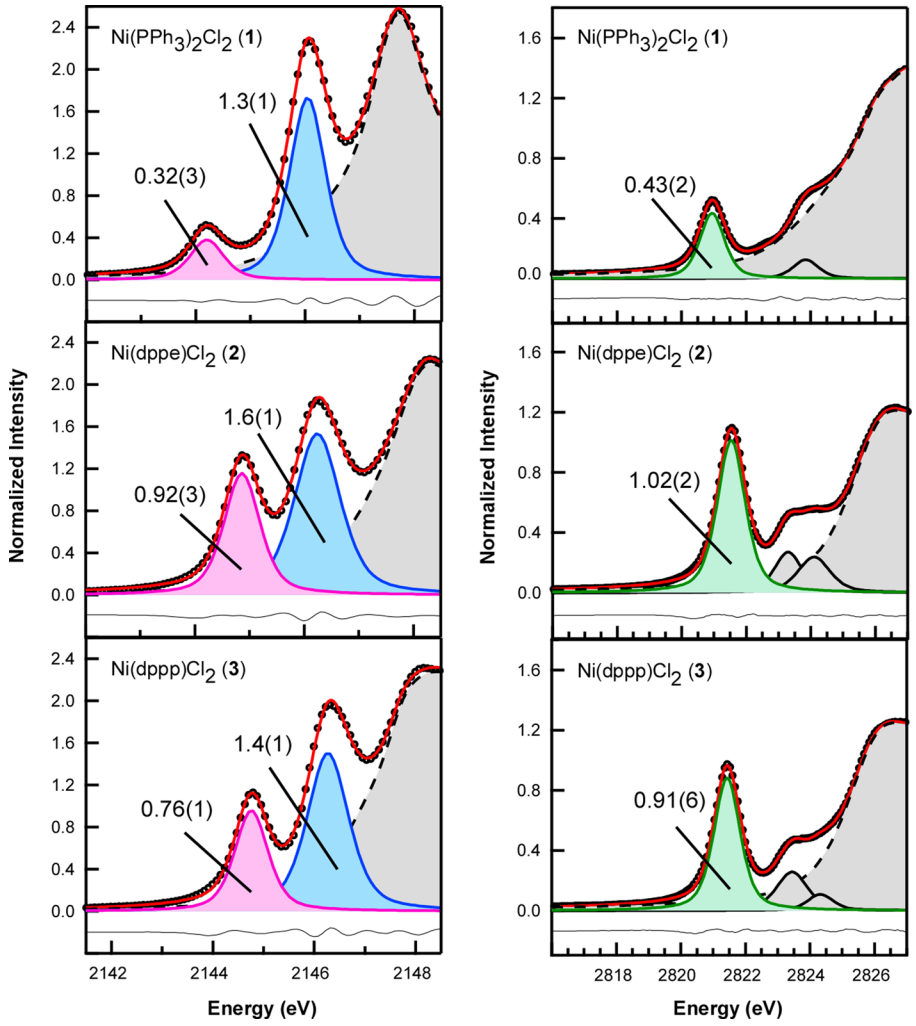

Figure 3. Truncated curve-fit models of the P K-edge (left) and Cl K-edge (right) XAS spectra for $Ni(PPh_3)_2Cl_2$ (**1**), $Ni(dppe)Cl_2$ (**2**), and $Ni(dppp)Cl_2$ (**3**). Full curve fits are located in Figure S11, Supporting Information.

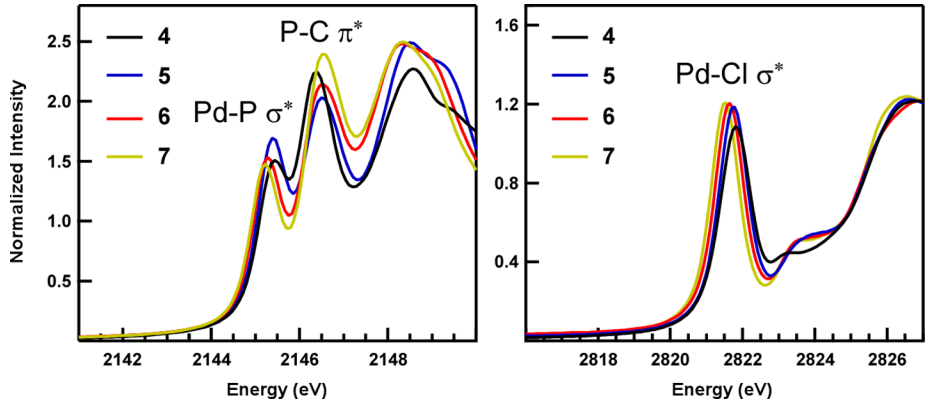

Figure 4. Normalized and background-subtracted P K-edge (left) and Cl K-edge (right) XAS spectra for $Pd(dppm)Cl_2$ (**4**; black), $Pd(dppe)Cl_2$ (**5**; blue), $Pd(dppp)Cl_2$ (**6**; red), and $Pd(dppb)Cl_2$ (**7**; gold).

minimum of four intensity values by two different researchers on each of two different samples so that reliable standard deviations could be determined.

The relative intensity of the first feature in the P K-edge XAS spectrum of **1** (1s → SOMO) is 0.32(3), which is significantly lower than the first feature's intensity in **2** and **3** (0.92(3) and 0.76(1), respectively). A similar relationship is observed in the Cl K-edge XAS data; the intensity of the first feature is 0.43(2) for **1**, whereas in **2** and **3** it is 1.02(2) and 0.91(6), respectively. As shown, the standard deviations associated with the first peaks were typically under 5%, whereas those for the second features were often 10% or greater. The increase in error for the higher energy features is attributed to their lower resolution and the presence of overlap on both sides of the curves.[59]

DOI: 10.1021/ic503125b
Inorg. Chem. 2015, 54, 5646−5659

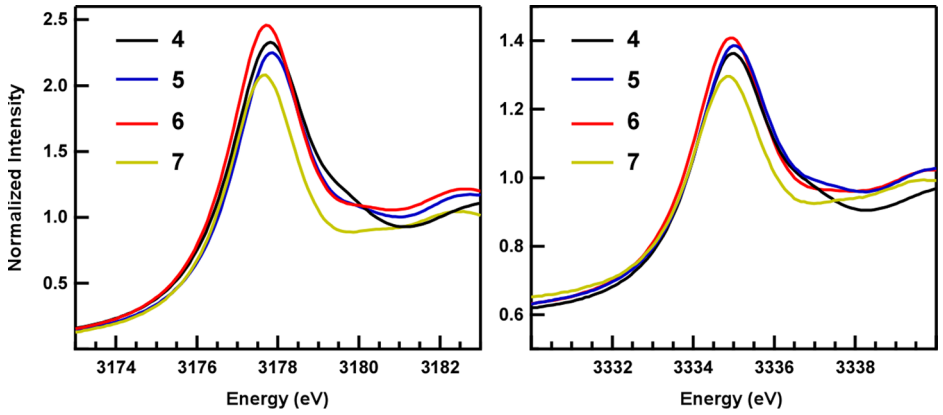

Figure 5. Normalized and background-subtracted Pd L_2-edge (right) and L_3-edge (left) XAS spectra for Pd(dppm)Cl_2 (**4**; black), Pd(dppe)Cl_2 (**5**; blue), Pd(dppp)Cl_2 (**6**; red), and Pd(dppb)Cl_2 (**7**; gold).

XAS Studies of Pd Diphosphine Complexes. To complement the analysis of the square planar Ni complexes **2** and **3** and to further evaluate how changes in diphosphine bite angle affect metal−ligand covalency, P K-edge, Cl K-edge, and Pd $L_{2/3}$-edge XAS data were collected on Pd(dppm)Cl_2 (**4**), Pd(dppe)Cl_2 (**5**), Pd(dppp)Cl_2 (**6**), and Pd(dppb)Cl_2 (**7**). The background-subtracted and normalized P and Cl K-edge data are shown in Figure 4, and the Pd L_2- and L_3-edge data are provided in Figure 5. The spectra have again been truncated to include the most important features, and the full spectra can be found in the Supporting Information (Figures S3 and S4). This series provided the opportunity to evaluate a broader range of bite angles by expanding the diphosphine library to include dppm and dppb in addition to the dppe and dppp discussed above. The experimental P−Pd−P bite angles—as obtained previously from single-crystal X-ray diffraction studies—increase stepwise across the series from 72.7° in **4** to 94.3° in **7**.[65,68] A similar trend was observed in the calculated structures (Table S1, Supporting Information).

The P and Cl K-edge XAS spectra of **4**−**7** have the same general profile as the isostructural Ni complexes **2** and **3**, but the pre-edge positions are shifted to higher energies (Table 1 and Figure S5, Supporting Information). The first features in the P K-edge spectra all occur between 2145.1 and 2145.4 eV and show subtle variations across the series. By comparison, the positions of the second peak in each of the three spectra are almost identical. A similar trend is observed in the Cl K-edge XAS spectra. The first pre-edge peaks occur at 2821.8 eV for **4** and **5** and slightly decrease in energy for **6** and **7** (2821.6 and 2821.5 eV, respectively). It should be noted that the relative differences in pre-edge positions for Pd(dppe)Cl_2 (**5**) and Pd(dppp)Cl_2 (**6**) are consistent with those observed in their isostructural Ni congeners **2** and **3**.

Using the method applied to the spectra of the Ni complexes, curve fits were used to model the P and Cl K-edge spectra of **4**−**7** (Figure 6). The intensities of the first P K-edge feature are identical in **4**, **6**, and **7** at 0.94(4), 0.94(3), and 0.92(9), but a 10% increase was observed in **5** at 1.06(4). A similar observation was made of the Cl K-edge spectra except that the Cl 1s → LUMO intensities are the same for **5**−**7** at 1.13(5), 1.14(6), and 1.12(5), respectively, whereas the feature in **4** was less intense at 1.00(4).

To investigate the electronic effects of bite angle variations from the perspective of the metal, Pd $L_{2/3}$-edge XAS spectra were collected for **4**−**7** (Figure 5). Transitions at the Pd L_2- and Pd L_3-edges are allowed Pd 2p → *n*d and involve the same metal−ligand MOs that give rise to pre-edge features in the ligand K-edge spectra. One resolved pre-edge feature is observed at each edge. The position of the Pd L_3-edge peaks, as determined from first- and second-derivative traces (Figure S6, Supporting Information), are all 3177.7 eV except in **5**, in which it is 0.1 eV higher. The Pd L_2-edge peaks follow at higher energy with closely matched positions at 3334.9 (**4**, **5**), 3334.8 (**6**), and 3345.0 eV (**7**). Interestingly, these Pd L_2 and L_3 pre-edge positions are approximately 2 eV higher than those in the square planar Pd(II) complex K_2PdCl_4.[80] This indicates a decrease in electron density at Pd in **4**−**7** and is consistent with replacing two chloride anions in $PdCl_4^{2-}$ with neutral diphosphine ligands.

XAS Studies of *trans*-Pd(PPh$_3$)$_2$Cl$_2$. P and Cl K-edge (Figures 7 and S7, Supporting Information) and Pd $L_{2/3}$-edge (Figure S8, Supporting Information) XAS data were collected on square planar *trans*-Pd$(PPh_3)_2Cl_2$ (**8**), which has trans phosphine and chloride ligands with Cl−Pd−Cl and P−Pd−P angles close to 180° (Figure 1). The P K-edge XAS spectrum of **8** reveals two resolved features at 2145.1 and 2146.2 eV and a broad third feature at higher energy. The position of the first feature is similar to those found in the *cis*-diphosphine complexes **4**−**7** (Table 1), but the curve-fit models indicate a substantial drop in intensity. This first feature was modeled with an area of 0.69(4), which is 35% smaller than that observed in the spectrum of **5**. Interestingly, the Cl K-edge XAS spectrum of **8** reveals an inverse trend. As in **4**−**7**, one dominant pre-edge feature is observable at 2821.5 eV. Modeling this pre-edge feature yielded an area of 1.51(3), which is 34% larger than the modeled feature in **5**. Also similar to **4**−**7** is the presence of one predominant peak in the Pd L_2- and L_3-edge XAS spectra of **8** (Figure S9, Supporting Information). The peak positions were located at 3334.5 and 3177.3 eV, respectively, which are both 0.3−0.5 eV lower than those observed in **4**−**7**.

Density Functional Theory Calculations and Molecular Structures. DFT was used to calculate gas-phase structures and evaluate the orbital manifold of **1**−**8**. These calculations utilized the B3LYP functional, which has been shown in previous studies to produce spectra that agree well with experiment despite its relative simplicity compared to most modern functionals.[52,53,57−60] Experimental bond distances and angles obtained from single-crystal X-ray diffraction experiments have been compiled in Table S1, Supporting

DOI: 10.1021/ic503125b
Inorg. Chem. 2015, 54, 5646−5659

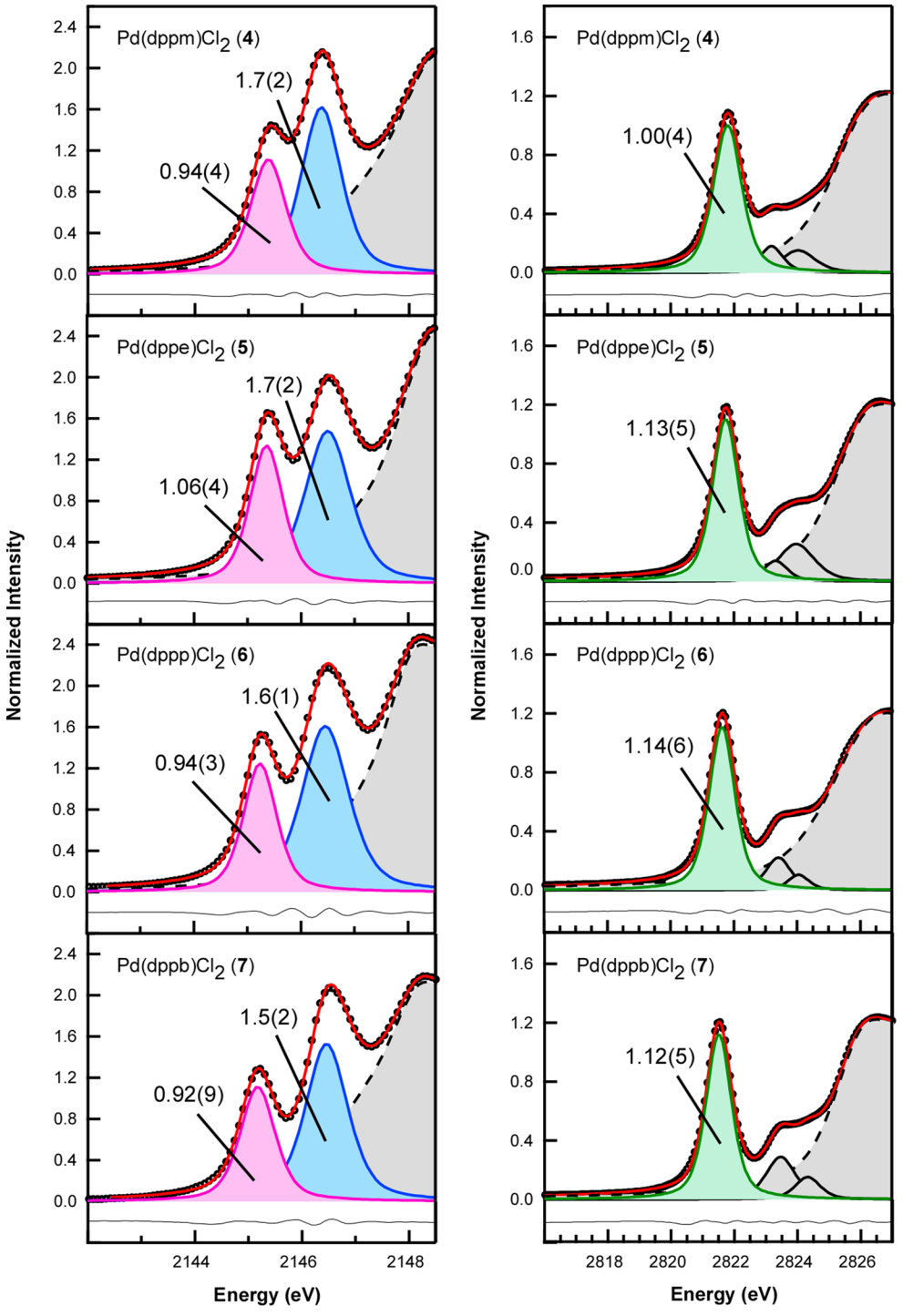

Figure 6. Curve-fit models of the P K-edge (left) and Cl K-edge (right) XAS spectra for Pd(dppm)Cl_2 (**4**), Pd(dppe)Cl_2 (**5**), Pd(dppp)Cl_2 (**6**), and Pd(dppb)Cl_2 (**7**). Full curve fits can be found in Figure S12, Supporting Information.

Information, with those obtained from the calculated structures. While calculations with B3LYP overestimate the bond distances and diphosphine bite angles, they reproduce the general trends observed in the solid-state structures. Orbital compositions most relevant to the interpretation of the XAS data are compiled in Table S2, Supporting Information, and these will be discussed in the following section with the TDDFT results. Please refer to the Experimental Section for a detailed discussion of the computational methodology.

DISCUSSION

Analysis of Coordination Geometry Variations. To account for the differences in the XAS spectra of the Ni complexes, it is useful to first consider how the different coordination geometries in **1** and **2** affect the molecular orbitals (MOs) and their associated electronic states. Despite the differences in geometry, the point group symmetry of **1** and **2** can be approximated as C_{2v} if only the atoms bound to Ni are considered. Ligand field diagrams for both complexes in C_{2v} symmetry have been described previously,[49,81,82] and we used

DOI: 10.1021/ic503125b
Inorg. Chem. 2015, 54, 5646−5659

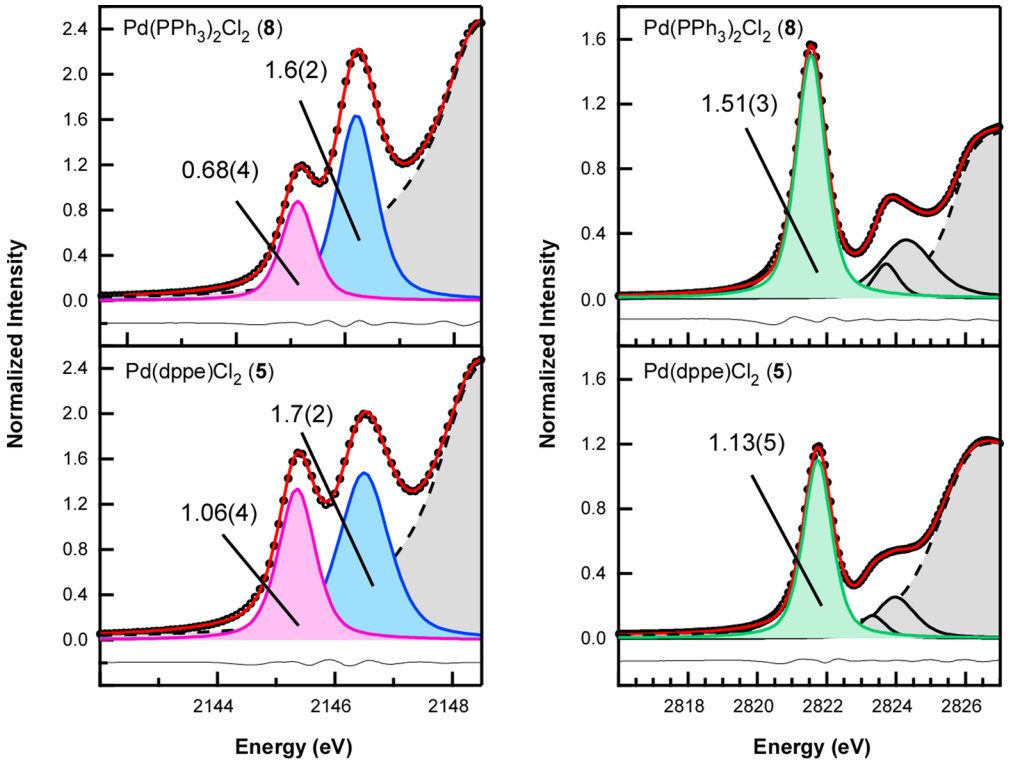

Figure 7. Curve-fit comparison of the P K-edge (left) and Cl K-edge (right) XAS spectra for *trans*-$Pd(PPh_3)_2Cl_2$ (**8**) and $Pd(dppe)Cl_2$ (**5**). Full curve fits can be found in Figure S12, Supporting Information.

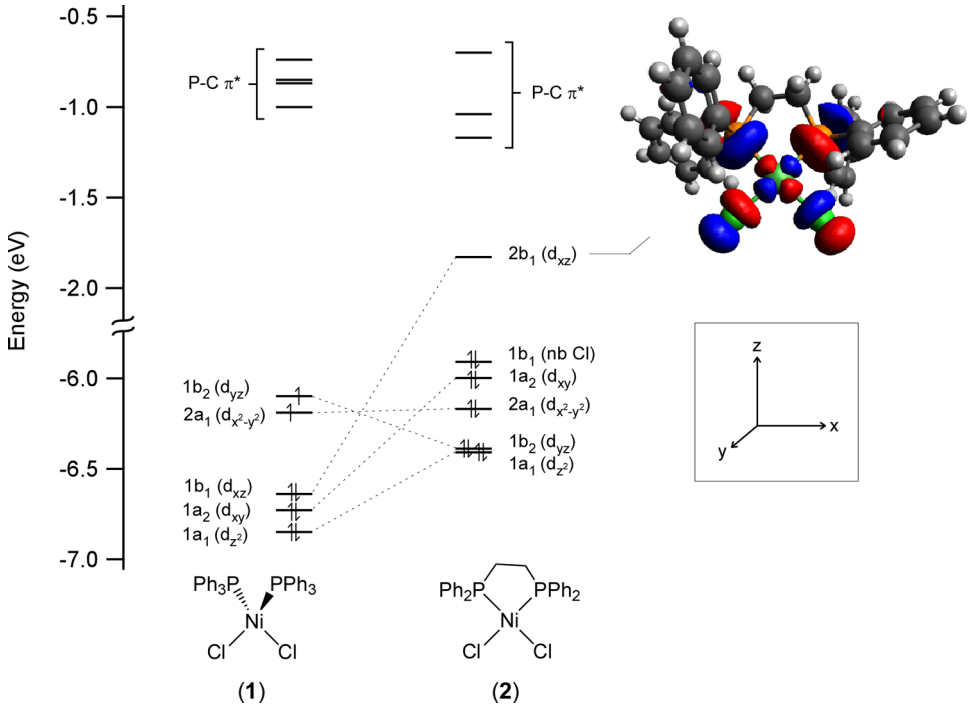

Figure 8. Truncated MO correlation diagram for $Ni(PPh_3)_2Cl_2$ (**1**) and $Ni(dppe)Cl_2$ (**2**). Point group symmetry is assigned as C_{2v} for both complexes, and labels correspond to those provided in Table S2, Supporting Information.

the DFT-derived Kohn–Sham orbitals and eigenvalues to quantify the MO energies and identify the higher lying MOs presented in the correlation diagram in Figure 8. Both complexes are d^8 (Ni^{2+}), but tetrahedral **1** is high spin with two singly occupied molecular orbitals (SOMOs), while square planar **2** is low spin with one unoccupied orbital located in the 3d manifold at higher energy. On the basis of this correlation diagram, the first feature in the P K-edge XAS spectrum of **1** can be assigned to transitions involving the SOMOs. Inspection of the Kohn–Sham orbitals revealed that the two SOMOs are a_1 and b_2 and contain mixing from Ni $3d_{x2-y2}$ and $3d_{yz}$. These symmetry assignments, along with those for the linear

DOI: 10.1021/ic503125b
Inorg. Chem. 2015, 54, 5646–5659

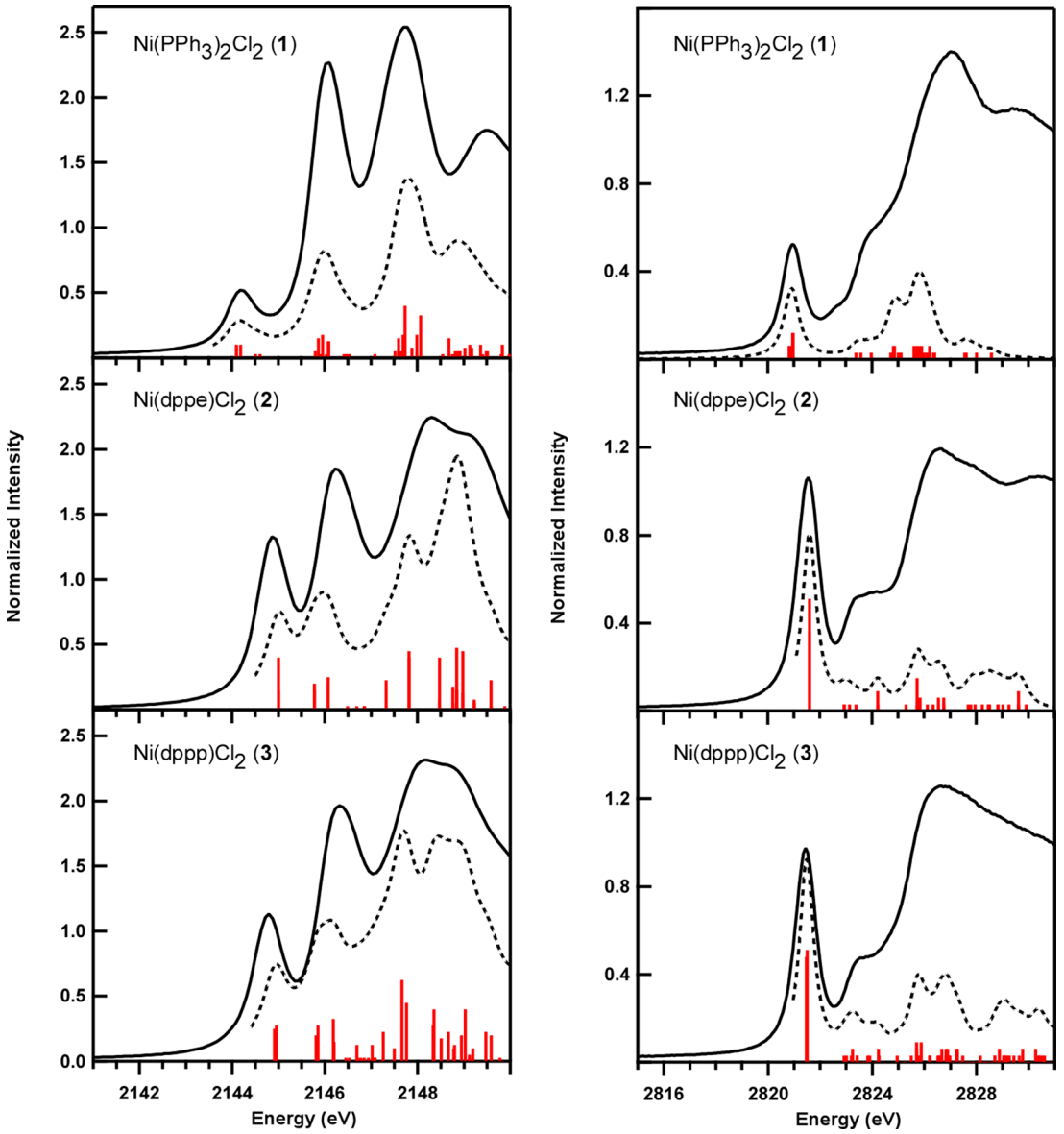

Figure 9. Comparison of the experimental and simulated P K-edge (left) and Cl K-edge (right) XAS spectra for $Ni(PPh_3)_2Cl_2$ (**1**), $Ni(dppe)Cl_2$ (**2**), and $Ni(dppp)Cl_2$ (**3**). Experimental spectra (solid lines), simulated spectra (dashed lines), and calculated transitions (red bars) are shown. Oscillator strengths have been multiplied by a factor of 250 for P and 300 for Cl to bring them on scale with the experimental data. An energy shift of +49.9 eV for P and +64.3 eV for Cl was applied to the calculated spectra of **1**, and a shift of +49.6 eV for P and +64.6 eV for Cl was applied to **2** and **3** so that the relative peak positions could be compared.

combinations of P 1s orbitals (a_1 and b_2), yield pairs of $^3B_2 \rightarrow {}^3B_2$ and $^3B_2 \rightarrow {}^3A_1$ transitions. The remaining pre-edge features in the P K-edge spectra involve excited states associated with the higher lying P−C π^* MOs. Similar assignments were made for the features in the Cl K-edge XAS spectrum. The linear combinations of Cl 1s orbitals (a_1 and b_1) and the two SOMOs in the d manifold yield allowed transitions of $^3B_2 \rightarrow {}^3B_2$, $^3B_2 \rightarrow {}^3A_1$, and $^3B_2 \rightarrow {}^3A_2$. The lack of intense pre-edge features at higher energy, such as those assigned to P−C π^* in the P K-edge spectrum, are consistent with the absence of additional antibonding MOs containing appreciable Cl 3p character.

The P and Cl K-edge XAS features in **2** and **3** yield assignments similar to those for **1**, except that metal-based transitions giving rise to the first peak in each spectrum involve the LUMO $2b_1$ (Figure 8). As a result of the change in spin multiplicity and the Cl and P atoms' residing in the same plane (XZ), the transitions in both spectra are assigned as $^1A_1 \rightarrow {}^1A_1$ and $^1A_1 \rightarrow {}^1B_1$. The transition assignments for **1**−**3** were corroborated by TDDFT calculations. The profiles and relative peak intensities of the simulated spectra are in agreement with the experimental data, and MO assignments were confirmed by natural transition orbital (NTO) analysis of the individual transitions (represented as bars in Figure 9).

Differences in the energy and intensity of the ligand K-edge XAS features in tetrahedral **1** and square planar **2** and **3** can be explained by considering how geometry change affects orbital overlap between the metal and the ligands. It is well established that the pseudotetrahedral geometry encountered in **1** yields a weak ligand field and relatively poor overlap between the frontier orbitals on the metal and ligands. A change to square planar geometry brings P and Cl into the plane of the Ni $3d_{xz}$ orbital, thereby yielding an increase in σ-type metal−ligand

DOI: 10.1021/ic503125b
Inorg. Chem. 2015, 54, 5646−5659

orbital overlap. The resulting increase in orbital mixing is clearly reflected by the increase in the intensity and energy of the first feature in the P and Cl K-edge XAS spectra for **2** and **3**. Similar results showing the impact of tetrahedral to square planar distortions on metal−chloride covalency have been well documented in Cl K-edge XAS studies of tetrachlorometalates.[50] We show here for the first time that the same phenomenon is observed in complexes containing phosphine and diphosphine ligands using P K-edge XAS.

Evaluation of Diphosphine Bite Angle Variations on Electronic Structure and Bonding. Unlike the large differences in the pre-edge positions and intensities for tetrahedral and square planar coordination complexes, differences in the XAS spectra of square planar Ni and Pd complexes were less pronounced. As shown in Table 1, the intensities of the first features in the P K-edge XAS spectra are identical within error for **4** (dppm), **6** (dppp), and **7** (dppb), but a 10% increase is observed for **5** (dppe). A similar increase in intensity is observed for Ni(dppe)Cl_2 (**2**) over Ni(dppp)Cl_2 (**3**). The first feature in each spectrum is assigned to P 1s → M−P σ^*, and its intensity reflects the amount of P 3p character mixing in the LUMO. DFT calculations were again used to quantify the energies and orbital compositions of the ground-state MOs for comparison to the XAS results. As observed in the P K-edge spectra, the ground-state calculations indicate that the % P 3p in the LUMO of **5** is approximately 10% greater than in the other three diphosphine complexes (Table S2, Supporting Information). TDDFT calculations further corroborate the increased peak intensity for **5** (Figure S10, Supporting Information). The sum of the calculated oscillator strength (f) for transitions associated with the first feature in each spectrum is 0.0022 (**4**), 0.0026 (**5**), 0.0024 (**6**), and 0.0022 (**7**). While at first glance the absolute differences appear to be insignificant, a calculated increase of 0.0002−0.0004 in **5** corresponds to an increase of 8−15%, which is consistent with the 10% increase observed in the experimental data.

To rationalize the P K-edge XAS results obtained for the diphosphine complexes **2**−**7**, we compared the spectroscopic intensities to variations in the experimental and calculated structures. While it is known that bond distances are not necessarily representative of variations in metal−ligand covalency,[83] the increase in M−P covalency for the dppe complexes **2** and **5** are consistent with M−P bond distances obtained from single-crystal X-ray diffraction (XRD) data. The average Ni−P bond distance for **2** is 0.03 Å less than in **3**, and the average Pd−P bond distance in **5** is 0.01−0.02 Å less than those in **4**, **6**, and **7** (Table S2, Supporting Information).[65,68,84,85]

Further analysis of the structural data for **4**−**7** indicated that the increased intensity of the 1s → LUMO transitions in the P K-edge XAS spectrum of Pd(dppe)Cl_2 could not be ascribed to it having a diphosphine bite angle closest to 90°. This is notable because calculated Walsh diagrams for square planar diphosphine complexes indicate a LUMO energy maximum close to 90°, suggesting that this may represent the preferred diphosphine bite angle for maximum M−P orbital overlap. Crystallographic data reported for **5** and **6** indicate that the bite angle in Pd(dppp)Cl_2 is closer to 90° (β = 90.6°) than Pd(dppe)Cl_2 (β = 85.8°).[65] Bite angle values from the DFT calculations reported here are more ambiguous because **5** and **6** both show similar bite angle deviations from 90°, albeit in the opposite direction (β = 87.5° and 94.5°, respectively). To show the trend more clearly, we plotted the calculated bite angle

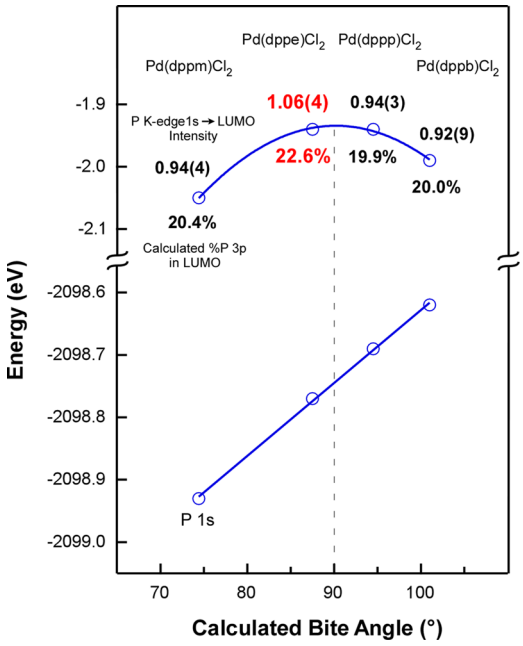

Figure 10. Calculated P 1s and LUMO energies of **4**−**7** as a function of the bite angle obtained from ground-state DFT calculations. Numbers above the LUMO energies indicate the experimental P K-edge 1s → LUMO intensities, and those below indicate the calculated % P 3p character in the LUMO. Dotted line represents a bite angle of 90° for reference.

against the LUMO and P 1s orbital energies for **4**−**7** in Figure 10. The variations in LUMO energies corroborate the known concave energy profile reported previously in Walsh diagrams of square planar diphosphine complexes.[42,48] As in previous reports, the energy maximum occurs close to a 90° bite angle, but it is clear that the P K-edge XAS intensity and calculated % P 3p character does not track with the change in LUMO energy. The P 1s energies are also included in the plot to explain why the experimental 1s → LUMO transition energies are similar in the XAS spectra of **4** and **5** but decrease for **6** and **7**. While the P 1s orbital energies increase linearly across the series with increasing bite angle, the concave LUMO energies maintain similar 1s → LUMO energy gaps for **4** and **5**, but the energy gap decreases sequentially for **6** and **7**.

It is not immediately clear what makes the dppe complexes **2** and **5** unique with respect to the other diphosphine complexes. There are two variables responsible for variations in metal−ligand covalency: frontier orbital energies and M−L orbital overlap.[49] Given that each diphosphine contains identical substituents attached to P, it seems unlikely that the difference in M−P covalency for the dppe complexes is a consequence of different frontier orbital energies. In light of the backbone changes, it appears more reasonable that the differences are a consequence of structure-induced variations in M−P orbital overlap.

One structural possibility we explored to account for the P K-edge XAS results for **2**−**7** were small dihedral distortions from square planar to tetrahedral geometry defined as twist angle.[32,33] The large changes in M−P covalency observed for tetrahedral **1** and square planar **2** suggested that smaller variations of this type may be influencing M−P covalency in the square planar diphosphine complexes. Structural data obtained from single-crystal XRD studies of the Pd complexes revealed that Pd(dppe)Cl_2, which has the greatest M−P covalency, does

DOI: 10.1021/ic503125b
Inorg. Chem. 2015, 54, 5646−5659

indeed have a smaller twist angle (3°) than **4**, **6**, and **7** (8–9°).[65,68,86] However, DFT and TDDFT calculations suggested that these differences have little impact on M–P orbital mixing. For example, increasing the twist angle of 1.8° in the calculated structure of **4** to the experimental value of 8.4° did not result in any change in the percent P 3p mixing in the LUMO or in the calculated oscillator strength of the first P K-edge feature. A similar calculation on **6**, in which the twist angle was reduced from 9.2° in the optimized ground-state structure to 0°, resulted in a small decrease in P 3p character in the LUMO from 20.8% to 19.8%. Finally, the twist angle was systematically changed in **5** from 0° to 45° in 5° increments. The resulting data again revealed a slight decrease in P 3p character as the twist angle was decreased from 45° (23.6%) to 0° (22.8%). Overall, the calculations suggest that the unique increase in P K-edge XAS intensity for **5** cannot simply be attributed to changes in twist angle.

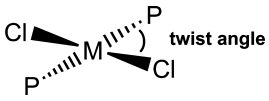

We are continuing to pursue additional data that will help us evaluate how other structural variations are affecting M–P covalency in square planar **2**–**7**. Our current hypothesis is that changes to the M–P–CH_2 angle in the diphosphine backbone is affecting orbital overlap between P lone pairs and d orbitals on the metal. As observed with bite angles, crystallographic data reported for **4**–**7** reveals that Pd–P–CH_2 angles increase stepwise from 94.7/94.4° (**4**) to 108.5/107.9° (**5**) to 116.0/115.6° (**6**) to 118.9/117.8° (**7**).[65,68] While more research is ultimately needed to determine how these angles compare to the orientation and positioning of the P lone pairs, especially with respect to the d orbitals on the metal,[38] it seems highly plausible that the M–P–CH_2 angles are implicated in the observed increase in M–P covalency for **2** and **5**.

Evaluation of Bite Angle Variations on M–Cl Bonding. The Cl K-edge XAS spectra collected for **4**–**7** show different trends in spectral intensity than do the P K-edge data. The first feature in the Cl K-edge XAS spectra reveals that there is no statistical difference in the modeled intensity for **5**–**7** (1.12–1.14), whereas a decrease to 1.00(4) is observed for **4**. DFT and TDDFT calculations are consistent, with **4** having the lowest intensity and the smallest amount of calculated Cl 3p character in the LUMO. However, the calculations indicate that the intensity should increase incrementally across the series instead of leveling off after **5** as the XAS data suggest. The inconsistencies between the DFT calculations and the XAS data, particularly for **5**–**7**, could be a consequence of the different bond metrics observed in the experimental and calculated structures. While bond angles involving Pd and P show matching trends in both experiment and theory, there are appreciable differences observed for those involving Cl. For example, the calculated Cl–P–Cl angles decrease stepwise from **4** (95.1°) to **7** (89.9°), but the experimental structures indicate that those in **4** and **5** are both close to 94°, while those in **6** and **7** are close to 90° (Table S1, Supporting Information). A similar difference is observed in the comparison of the calculated and experimental structures for the Ni complexes **2** and **3**.

Given the apparent lack of correlation between structural metrics and Cl 3p mixing, it does not appear that there is a stereoelectronic explanation that accounts for the differences between **4** and **5**–**7**. This is perhaps not too surprising given that there are no structural constraints associated with terminal chloride ligands to affect how the frontier orbitals overlap. Unlike the diphosphines, which have alkane backbones that can affect the orientation of the P lone pairs, the terminal chloride ligands are spherical. While further studies will be needed to account for the precise factors influencing Pd–Cl covalency, it is clear that **4** has the least covalent Pd–Cl mixing.

XAS Comparison of Isostructural Ni and Pd Complexes. The XAS data collected for the square planar Ni and Pd complexes provided an opportunity to determine how changing the identity of the metal affects metal–ligand covalency and 1s → LUMO transition energies. The P and Cl K-edge XAS data revealed that the 1s → LUMO features for the Pd complexes **5** and **6** are higher energy and have greater intensity than their isostructural Ni congeners **2** and **3**. Starting with transition energies, the pre-edge features in the P K-edge XAS spectra of **5** and **6** are 0.4–0.5 eV higher in energy. An increase in energy is also observed in the Cl K-edge spectra, but the shift is less pronounced (0.2 eV). The DFT calculations suggest that the origin of the ∼0.4 eV increase in the energy in the P K-edge transitions for the Pd complexes can be attributed to a combination of the 1s orbitals dropping in energy by 0.2 eV and a 0.2 eV increase in the energy of the LUMO (Table S2, Supporting Information). By comparison, the shifts in the energy of the complementary Cl K-edge features are attributed almost exclusively to changes in the energy of the LUMO because the energy of the Cl 1s orbitals in the Ni and Pd complexes are almost identical.

Differences in the energy of the 1s orbitals are known to be heavily dependent on the effective nuclear charge (Z_{eff}) of the coordinated metal. The observed changes in the P 1s orbital energies from Ni^{2+} to Pd^{2+} are consistent with the known increase in Z_{eff} going from a first-row to a second-row metal. As Z_{eff} increases, the ligand 1s orbitals become more stabilized (i.e., decrease in energy), which results in 1s → σ^* transitions that are higher in energy. It appears that the P 1s orbitals are more susceptible to the changes in Z_{eff} than they are in Cl, which is consistent with previous experimental data showing that M–Cl bonds are more ionic (i.e., less covalent) than M–P bonds.[42]

The modeled intensity of the 1s → σ^* transitions in the P and Cl K-edge spectra of the Pd complexes is significantly greater in the Pd complexes than in their Ni congeners. Comparison of **2** and **5**, which both contain dppe, revealed intensity values of 0.92(3) and 1.06(4) for the P K-edge data and 1.02(2) and 1.13(5) in the Cl K-edge data for **2** and **5**, respectively. A similar observation is made for the dppp complexes **3** and **6** (Table 1). The observed intensity increase for Pd is consistent with the expected increase in metal–ligand covalency for 4d vs 3d metals. The higher covalency is attributed to increased metal–ligand orbital overlap that results from the greater radial extension of the 4d orbitals in Pd.

XAS Analysis of the Trans Influence in *trans*-Pd(PPh_3)$_2$$Cl_2$. Exchanging the diphosphine ligands in **4**–**7** for two monodentate PPh_3 ligands yields a square planar complex with the phosphine ligands positioned trans to one another. This afforded an opportunity to explore variations in metal–ligand covalency associated with the trans influence of phosphine and chloride ligands. The trans influence,[87] also known as the structural trans effect,[88] is a well-known phenomenon in coordination chemistry. It defines the weakening of metal–ligand bonds located in the trans position in ground-state structures. Most of what is known about the trans influence

DOI: 10.1021/ic503125b
Inorg. Chem. 2015, 54, 5646–5659

comes from structural data obtained from single-crystal X-ray diffraction studies. Bond length variations caused by different trans ligands have been used to rank ligands empirically in order of increasing trans influence. Spectroscopic methods such as NMR and IR spectroscopy have also been used, but it can be harder to glean reliable information via these methods because of other variables that contribute to NMR shifts and the coupling of vibrational modes.[88]

Despite long-standing knowledge of the trans influence, its origin continues to be investigated. Burdett and Albright analyzed potential trans-influence contributions using molecular orbital theory and the angular overlap method.[89] Their findings suggested that there are two key orbital contributions to the trans influence. They noted that both may be important but suggested that the magnitude of their importance was system dependent. First, they mathematically derived the dependence of M−L orbital mixing on the overlap integral and energies of different trans ligands. This contribution to the trans influence can be thought of as unequal sharing of the same d orbital between two different trans ligands. Second, they described how mixing between occupied MOs containing metal p character and virtual MOs containing metal d character can lead to preferential weakening of one of the trans ligand bonds. The repulsive nature of the second effect was also described recently by Pinter and co-workers in theoretical studies of *trans*-$XPtCl_2NH_3$, where X = NH_3, PH_3, CO, and C_2H_4.[90] As the name implies, it has been suggested that the effect is assigned to Pauli repulsion that propagates through filled MOs containing metal p character. The occupied MOs mix with the LUMO, which subsequently allows strong σ-donor ligands to destabilize opposing ligands in the trans position.[90]

The Cl and P K-edge XAS results both show large changes in the intensity of the 1s → σ^* transitions, which indicate corresponding differences in M−L covalency. The changes are consistent with empirically derived trends in the trans influence. The trans ligands in $Pd(PPh_3)_2Cl_2$ are identical (Cl···Cl and P···P) so there is equal sharing (and/or repulsion) of electron density across the d-orbital lobes. When the phosphines are moved trans to chloride ligands in $Pd(dppe)Cl_2$, we see a reduction in M−Cl orbital mixing and an increase in M−P orbital mixing. This is expected given that phosphines are known to have a stronger trans influence than chloride. Coincidentally, though the change in M−P and M−Cl intensity is in opposite directions, the absolute magnitude of the change for Cl and P is identical within error (Δ_{Cl} = −0.37; Δ_P = +0.38).

CONCLUDING REMARKS

In summary, we demonstrated how ligand K-edge XAS in combination with DFT and TDDFT can be used to evaluate the impact of coordination geometry, bite angle, and trans influence on metal−ligand covalency in phenyl-substituted phosphine and diphosphine complexes. Ni−P and Ni−Cl covalency more than doubled when the coordination geometry in tetrahedral $Ni(PPh_3)_2Cl_2$ (**1**) was changed to square planar $Ni(dppe)Cl_2$ (**2**). By comparison, the impact of bite angle on the P K-edge XAS spectra of square planar diphosphine complexes **2**−**7** was significantly less pronounced. However, a remarkable increase in M−P covalency was observed in the dppe complexes **2** and **5**, and the experimental results were corroborated by DFT and TDDFT calculations. As a final analysis, we quantified changes in M−P and M−Cl covalency associated with the trans influence. XAS comparisons of *trans*-$Pd(PPh_3)_2Cl_2$ (**8**) and the cis diphosphine complexes **4**−**7** showed large differences in Pd−P and Pd−Cl covalency consistent with empirical trends in trans influence.

Despite long-standing discussions about the presence, magnitude, and origin of electronic bite angle dependence in diphosphine complexes, we found that bite angle alone does not account for orbital-mixing variations in the square planar diphosphine complexes **2**−**7**. The XAS and DFT data showed that the energy of the LUMO varied with bite angle as expected, but the LUMO energies were not representative of changes in M−P covalency. The decoupling of LUMO energies, which are highly dependent on P−M−P bite angles, and M−P covalency, which is not, suggests that other structural parameters may be more important when evaluating overlap contributions to covalent diphosphine bonding with Ni and Pd. Furthermore, it appears likely that spatial overlap between the phosphorus lone pairs and the metal d orbitals is governed by some combination of structural metrics that include M−P−C angles. Lichtenberger proposed this idea over two decades ago in his description of "phosphine twist", which was described as the bending of metal−phosphine bonds to maximize overlap between frontier orbitals on the metal and ligand.[38] He used this concept to account for the lack of bite angle correlations to photoelectron spectroscopy data collected on the same Pd complexes studied here.[38] The P K-edge XAS results for **2**−**7** corroborate Lichtenberger's findings and suggest that phosphine twist or a conceptually similar orbital overlap model may indeed account for differences in M−P covalency as the backbone is modified in alkane-bridged diphosphines. We are now exploring this possibility by collecting P K-edge XAS data on other transition metal diphosphine complexes to determine if structural changes to the diphosphine backbone can be modeled to account for variations in M−P covalency.

ASSOCIATED CONTENT

Supporting Information

Complete ref 70, complete XAS spectra, first- and second-derivative traces, and complete curve fits; simulated XAS spectra of **4**−**8** from TDDFT; calculated MO compositions and energies, atomic coordinates, and Mulliken charges; comparison of experimental and calculated bond distances and angles. The Supporting Information is available free of charge on the ACS Publications website at DOI: 10.1021/ic503125b.

AUTHOR INFORMATION

Corresponding Authors

*E-mail: jkeith@colgate.edu.
*E-mail: scott-daly@uiowa.edu.

Author Contributions

All authors have given approval to the final version of the manuscript.

Notes

The authors declare no competing financial interest.

ACKNOWLEDGMENTS

This work was generously supported by the University of Iowa (SRD), the George Washington University (SRD), and Colgate University (JMK). This work was also supported by Western Illinois University's College of Arts and Science Undergraduate Research Awards (BJB). JMK would like to thank Patrick Holloway of Colgate University for high-performance computing support. Portions of this research were carried out at the

DOI: 10.1021/ic503125b
Inorg. Chem. 2015, 54, 5646−5659

Stanford Synchrotron Radiation Laboratory (SSRL), which is a national user facility supported by the U.S. Department of Energy, Office of Basic Energy Sciences.

REFERENCES

(1) In *Phosphorus(III) Ligands in Homogeneous Catalysis: Design and Synthesis*; Kamer, P. C. J., van Leeuwen, P. W. N. M., Eds.; Wiley: West Sussex, 2012.
(2) Allen, D. W. *Organophosphorus Chem.* **2011**, *40*, 1−51.
(3) Golovin, M. N.; Rahman, M. M.; Belmonte, J. E.; Giering, W. P. *Organometallics* **1985**, *4*, 1981−1991.
(4) Drago, R. S.; Joerg, S. *J. Am. Chem. Soc.* **1996**, *118*, 2654−2663.
(5) Joerg, S.; Drago, R. S.; Sales, J. *Organometallics* **1998**, *17*, 589−599.
(6) Wilson, M. R.; Prock, A.; Giering, W. P.; Fernandez, A. L.; Haar, C. M.; Nolan, S. P.; Foxman, B. M. *Organometallics* **2002**, *21*, 2758−2763.
(7) Kuehl, O. *Coord. Chem. Rev.* **2005**, *249*, 693−704.
(8) Mampa, R. M.; Fernandes, M. A.; Carlton, L. *Organometallics* **2014**, *33*, 3283−3299.
(9) Tolman, C. A. *J. Am. Chem. Soc.* **1970**, *92*, 2953−2956.
(10) Tolman, C. A. *Chem. Rev.* **1977**, *77*, 313−348.
(11) Mukerjee, S. L.; Nolan, S. P.; Hoff, C. D.; Lopez de la Vega, R. *Inorg. Chem.* **1988**, *27*, 81−85.
(12) Smith, D. C., Jr.; Haar, C. M.; Stevens, E. D.; Nolan, S. P.; Marshall, W. J.; Moloy, K. G. *Organometallics* **2000**, *19*, 1427−1433.
(13) Fey, N.; Harvey, J. N.; Lloyd-Jones, G. C.; Murray, P.; Orpen, A. G.; Osborne, R.; Purdie, M. *Organometallics* **2008**, *27*, 1372−1383.
(14) Fey, N.; Orpen, A. G.; Harvey, J. N. *Coord. Chem. Rev.* **2009**, *253*, 704−722.
(15) Jover, J.; Fey, N.; Harvey, J. N.; Lloyd-Jones, G. C.; Orpen, A. G.; Owen-Smith, G. J. J.; Murray, P.; Hose, D. R. J.; Osborne, R.; Purdie, M. *Organometallics* **2012**, *31*, 5302−5306.
(16) Jover, J.; Fey, N. *Dalton Trans.* **2013**, *42*, 172−181.
(17) Dierkes, P.; van Leeuwen, P. W. N. M. *J. Chem. Soc., Dalton Trans.* **1999**, 1519−1530.
(18) Kamer, P. C. J.; van Leeuwen, P. W. N. M.; Reek, J. N. H. *Acc. Chem. Res.* **2001**, *34*, 895−904.
(19) Birkholz, M.-N.; Freixa, Z.; van Leeuwen, P. W. N. M. *Chem. Soc. Rev.* **2009**, *38*, 1099−1118.
(20) Freixa, Z.; Van Leeuwen, P. W. N. M. *Dalton Trans.* **2003**, 1890−1901.
(21) Van Leeuwen, P. W. N. M.; Kamer, P. C. J.; Reek, J. N. H. *Pure Appl. Chem.* **1999**, *71*, 1443−1452.
(22) In contrast to natural bite angle, which is defined as the same angle in the absence of metal influences, see: Casey, C. P.; Whiteker, G. P. *Isr. J. Chem.* **1990**, *30*, 299−304. Dierkes, P.; van Leeuwen, P. W. N. M. *J. Chem. Soc., Dalton Trans.* **1999**, 1519−1530. Kuhl, O. *Can. J. Chem.* **2007**, *85*, 230−238.
(23) Tatsumi, K.; Hoffmann, R.; Yamamoto, A.; Stille, J. K. *Bull. Chem. Soc. Jpn.* **1981**, *54*, 1857−1867.
(24) Mann, G.; Baranano, D.; Hartwig, J. F.; Rheingold, A. L.; Guzei, I. A. *J. Am. Chem. Soc.* **1998**, *120*, 9205−9219.
(25) Marcone, J. E.; Moloy, K. G. *J. Am. Chem. Soc.* **1998**, *120*, 8527−8528.
(26) Korenaga, T.; Abe, K.; Ko, A.; Maenishi, R.; Sakai, T. *Organometallics* **2010**, *29*, 4025−4035.
(27) Anstaett, P.; Schoenebeck, F. *Chem.—Eur. J.* **2011**, *17* (12340−12346), S12340/12341−S12340/12379.
(28) Gathy, T.; Riant, O.; Peeters, D.; Leyssens, T. *J. Organomet. Chem.* **2011**, *696*, 3425−3430.
(29) Brown, J. M.; Guiry, P. J. *Inorg. Chim. Acta* **1994**, *220*, 249−259.
(30) Zuidema, E.; van Leeuwen, P. W. N. M.; Bo, C. *Organometallics* **2005**, *24*, 3703−3710.
(31) Saidi, O.; Liu, S.; Xiao, J. *J. Mol. Catal. A: Chem.* **2009**, *305*, 130−134.
(32) van Zeist, W.-J.; Visser, R.; Bickelhaupt, F. M. *Chem.—Eur. J.* **2009**, *15*, 6112−6115.
(33) van Zeist, W.-J.; Bickelhaupt, F. M. *Org. Biomol. Chem.* **2010**, *8*, 3118−3127.
(34) van Zeist, W.-J.; Bickelhaupt, F. M. *Dalton Trans.* **2011**, *40*, 3028−3038.
(35) Fernandez, I.; Bickelhaupt, F. M. *Chem. Soc. Rev.* **2014**, *43*, 4953−4967.
(36) Frenking, G.; Wichmann, K.; Frohlich, N.; Loschen, C.; Lein, M.; Frunzke, J.; Rayon, V. M. *Coord. Chem. Rev.* **2003**, *238*−*239*, 55−82.
(37) Bancroft, G. M.; Dignard-Bailey, L.; Puddephatt, R. J. *Inorg. Chem.* **1986**, *25*, 3675−3680.
(38) Lichtenberger, D. L.; Jatcko, M. E. *J. Coord. Chem.* **1994**, *32*, 79−101.
(39) Angermund, K.; Baumann, W.; Dinjus, E.; Fornika, R.; Goerls, H.; Kessler, M.; Krueger, C.; Leitner, W.; Lutz, F. *Chem.—Eur. J.* **1997**, *3*, 755−764.
(40) DePriest, J.; Zheng, G. Y.; Woods, C.; Rillema, D. P.; Mikirova, N. A.; Zandler, M. E. *Inorg. Chim. Acta* **1997**, *264*, 287−296.
(41) Crotti, C.; Farnetti, E.; Celestino, T.; Stener, M.; Fontana, S. *Organometallics* **2004**, *23*, 5219−5225.
(42) Tromp, M.; van Bokhoven Jeroen, A.; van Strijdonck Gino, P. F.; van Leeuwen Piet, W. N. M.; Koningsberger Diek, C.; Ramaker David, E. *J. Am. Chem. Soc.* **2005**, *127*, 777−789.
(43) Miedaner, A.; Haltiwanger, R. C.; DuBois, D. L. *Inorg. Chem.* **1991**, *30*, 417−427.
(44) Nimlos, M. R.; Chang, C. H.; Curtis, C. J.; Miedaner, A.; Pilath, H. M.; DuBois, D. L. *Organometallics* **2008**, *27*, 2715−2722.
(45) Abukari, M. A.; Suzuki, T.; Kita, M. *Polyhedron* **2013**, *52*, 364−369.
(46) Massera, C.; Frenking, G. *Organometallics* **2003**, *22*, 2758−2765.
(47) Flener Lovitt, C.; Frenking, G.; Girolami, G. S. *Organometallics* **2012**, *31*, 4122−4132.
(48) Nikolov, G. S. *J. Inorg. Nucl. Chem.* **1977**, *39*, 249−253.
(49) Albright, T. A.; Burdett, J. K.; Whangbo, M. H. *Orbital Interactions in Chemistry*; Wiley-Interscience: New York, 1985.
(50) Solomon, E. I.; Hedman, B.; Hodgson, K. O.; Dey, A.; Szilagyi, R. K. *Coord. Chem. Rev.* **2005**, *249*, 97−129.
(51) Heitler, W.; London, F. *Z. Phys.* **1927**, *44*, 455−472.
(52) Minasian, S. G.; Keith, J. M.; Batista, E. R.; Boland, K. S.; Clark, D. L.; Conradson, S. D.; Kozimor, S. A.; Martin, R. L.; Schwarz, D. E.; Shuh, D. K.; Wagner, G. L.; Wilkerson, M. P.; Wolfsberg, L. E.; Yang, P. *J. Am. Chem. Soc.* **2012**, *134*, 5586−5597.
(53) Loble, M. W.; Keith, J. M.; Altman, A. B.; Stieber, S. C. E.; Batista, E. R.; Boland, K. S.; Conradson, S. D.; Clark, D. L.; Lezama Pacheco, J.; Kozimor, S. A.; Martin, R. L.; Minasian, S. G.; Olson, A. C.; Scott, B. L.; Shuh, D. K.; Tyliszczak, T.; Wilkerson, M. P.; Zehnder, R. A. *J. Am. Chem. Soc.* **2015**, *137*, 2506−2523.
(54) Queen, M. S.; Towey, B. D.; Murray, K. A.; Veldkamp, B. S.; Byker, H. J.; Szilagyi, R. K. *Coord. Chem. Rev.* **2013**, *257*, 564−578.
(55) Recent publications: (a) Chandrasekaran, P.; Greene, A. F.; Lillich, K.; Capone, S.; Mague, J. T.; DeBeer, S.; Donahue, J. P. *Inorg. Chem.* **2014**, *53*, 9192−9205. (b) Pollock, C. J.; Tan, L. L.; Zhang, W.; Lancaster, K. M.; Lee, S. C.; DeBeer, S. *Inorg. Chem.* **2014**, *53*, 2591−2597. (c) Giles, L. J.; Grigoropoulos, A.; Szilagyi, R. K. *J. Phys. Chem. A* **2012**, *116*, 12280−12298. (d) Yan, Y.; Keating, C.; Chandrasekaran, P.; Jayarathne, U.; Mague, J. T.; DeBeer, S.; Lancaster, K. M.; Sproules, S.; Rubtsov, I. V.; Donahue, J. P. *Inorg. Chem.* **2013**, *52*, 6743−6751. (e) Sarangi, R.; Yang, L.; Winikoff, S. G.; Gagliardi, L.; Cramer, C. J.; Tolman, W. B.; Solomon, E. I. *J. Am. Chem. Soc.* **2011**, *133*, 17180−17191. (f) Silver, S. C.; Gardenghi, D. J.; Naik, S. G.; Shepard, E. M.; Huynh, B. H.; Szilagyi, R. K.; Broderick, J. B. *J. Biol. Inorg. Chem.* **2014**, *19*, 465−483.
(56) Kozimor, S. A.; Yang, P.; Batista, E. R.; Boland, K. S.; Burns, C. J.; Christensen, C. N.; Clark, D. L.; Conradson, S. D.; Hay, P. J.; Lezama, J. S.; Martin, R. L.; Schwarz, D. E.; Wilkerson, M. P.; Wolfsberg, L. E. *Inorg. Chem.* **2008**, *47*, 5365−5371.
(57) Daly, S. R.; Keith, J. M.; Batista, E. R.; Boland, K. S.; Clark, D. L.; Kozimor, S. A.; Martin, R. L. *J. Am. Chem. Soc.* **2012**, *134*, 14408−14422.

DOI: 10.1021/ic503125b
Inorg. Chem. 2015, 54, 5646−5659

(58) Spencer, L. P.; Yang, P.; Minasian, S. G.; Jilek, R. E.; Batista, E. R.; Boland, K. S.; Boncella, J. M.; Conradson, S. D.; Clark, D. L.; Hayton, T. W.; Kozimor, S. A.; Martin, R. L.; MacInnes, M. M.; Olson, A. C.; Scott, B. L.; Shuh, D. K.; Wilkerson, M. P. *J. Am. Chem. Soc.* **2013**, *135*, 2279−2290.
(59) Donahue, C. M.; Lezama Pacheco, J. S.; Keith, J. M.; Daly, S. R. *Dalton Trans.* **2014**, *43*, 9189−9201.
(60) Olson, A. C.; Keith, J. M.; Batista, E. R.; Boland, K. S.; Daly, S. R.; Kozimor, S. A.; MacInnes, M. M.; Martin, R. L.; Scott, B. L. *Dalton Trans.* **2014**, *43*, 17283−17295.
(61) Adhikari, D.; Mossin, S.; Basuli, F.; Huffman, J. C.; Szilagyi, R. K.; Meyer, K.; Mindiola, D. J. *J. Am. Chem. Soc.* **2008**, *130*, 3676−3682.
(62) Mossin, S.; Tran, B. L.; Adhikari, D.; Pink, M.; Heinemann, F. W.; Sutter, J.; Szilagyi, R. K.; Meyer, K.; Mindiola, D. J. *J. Am. Chem. Soc.* **2012**, *134*, 13651−13661.
(63) Shearer, J.; Callan, P. E.; Masitas, C. A.; Grapperhaus, C. A. *Inorg. Chem.* **2012**, *51*, 6032−6045.
(64) Venanzi, L. M. *J. Chem. Soc.* **1958**, 719−724.
(65) Steffen, W. L.; Palenik, G. J. *Inorg. Chem.* **1976**, *15*, 2432−2439.
(66) Miyaura, N.; Suzuki, A. *Org. Synth.* **1990**, *68*, 130−137.
(67) Sanger, A. R. *J. Chem. Soc., Dalton Trans.* **1977**, 1971−1976.
(68) Makhaev, V. D.; Dzhabieva, Z. M.; Konovalikhin, S. V.; D'Yachenko, O. A.; Belov, G. P. *Russ. J. Coord. Chem.* **1996**, *22*, 563−567.
(69) Ravel, B.; Newville, M. *J. Synchrotron Radiat.* **2005**, *12*, 537−541.
(70) Frisch, M. J. et al. *Gaussian 09*, Revision B.01; Gaussian, Inc.: Wallingford, CT, 2009. The full reference can be found in the Supporting Information.
(71) Lee, C.; Yang, W.; Parr, R. G. *Phys. Rev. B: Condens. Matter* **1988**, *37*, 785−789.
(72) Becke, A. D. *J. Chem. Phys.* **1993**, *98*, 5648−5652.
(73) Hay, P. J.; Wadt, W. R. *J. Chem. Phys.* **1985**, *82*, 299−310.
(74) Roy, L. E.; Hay, P. J.; Martin, R. L. *J. Chem. Theory Comput.* **2008**, *4*, 1029−1031.
(75) Hehre, W. J.; Ditchfield, R.; Pople, J. A. *J. Chem. Phys.* **1972**, *56*, 2257−2261.
(76) Hariharan, P. C.; Pople, J. A. *Theor. Chim. Acta* **1973**, *28*, 213−222.
(77) Elliott, P.; Furche, F.; Burke, K. *Rev. Comput. Chem.* **2009**, *26*, 91−165.
(78) Ellis, J. K.; Martin, R. L.; Scuseria, G. E. *J. Chem. Theory Comput.* **2013**, *9*, 2857−2869.
(79) Martin, R. L. *J. Chem. Phys.* **2003**, *118*, 4775−4777.
(80) Boysen, R. B.; Szilagyi, R. K. *Inorg. Chim. Acta* **2008**, *361*, 1047−1058.
(81) Fereday, R. J.; Hathaway, B. J.; Dudley, R. J. *J. Chem. Soc. A* **1970**, 571−574.
(82) Krzystek, J.; Park, J.-H.; Meisel, M. W.; Hitchman, M. A.; Stratemeier, H.; Brunel, L.-C.; Telser, J. *Inorg. Chem.* **2002**, *41*, 4478−4487.
(83) Minasian, S. G.; Krinsky, J. L.; Arnold, J. *Chem.—Eur. J.* **2011**, *17* (12234−12245), S12234/12231−S12234/12236.
(84) Ferguson, G.; McCrindle, R.; McAlees, A. J.; Parvez, M. *Acta Crystallogr., Sect. B* **1982**, *B38*, 2679−2681.
(85) Bomfim, J. A. S.; de Souza, F. P.; Filgueiras, C. A. L.; de Sousa, A. G.; Gambardella, M. T. P. *Polyhedron* **2003**, *22*, 1567−1573.
(86) Twist angles were determined by calculating the angle between the plane define by the P−M−P atoms and the plane defined by the Cl−M−Cl using Mercury CSD 3.5.1: Macrae, C. F.; Bruno, I. J.; Chisholm, J. A.; Edgington, P. R.; McCabe, P.; Pidcock, E.; Rodriguez-Monge, L.; Taylor, R.; van de Streek, J.; Wood, P. A. *J. Appl. Crystallogr.* **2008**, *41*, 466−470.
(87) Appleton, T. G.; Clark, H. C.; Manzer, L. E. *Coord. Chem. Rev.* **1973**, *10*, 335−422.
(88) Coe, B. J.; Glenwright, S. J. *Coord. Chem. Rev.* **2000**, *203*, 5−80.
(89) Burdett, J. K.; Albright, T. A. *Inorg. Chem.* **1979**, *18*, 2112−2120.
(90) Pinter, B.; Van Speybroeck, V.; Waroquier, M.; Geerlings, P.; De Proft, F. *Phys. Chem. Chem. Phys.* **2013**, *15*, 17354−17365.

DOI: 10.1021/ic503125b
Inorg. Chem. 2015, 54, 5646−5659